THE SHAPE OF THE TILTED MAGNETOPAUSE

W. P. OLSON

A Reprint from

NOVEMBER 1, 1969

Journal of Geophysical Research

VOLUME 74 NUMBER 24

PUBLISHED BY
THE AMERICAN GEOPHYSICAL UNION

JOURNAL OF GEOPHYSICAL RESEARCH, SPACE PHYSICS VOL. 74, NO. 24, NOVEMBER 1, 1969

The Shape of the Tilted Magnetopause[1]

W. P. OLSON[2]

Department of Planetary and Space Science
University of California, Los Angeles, California 90024

A model for the determination of the shape of the magnetopause is developed that permits the inclusion of cases where the solar wind is directed obliquely toward the geomagnetic dipole axis. The solar wind is assumed to have no motions perpendicular to its (constant) velocity vector (zero temperature approximation) and to be free of magnetic fields. The region within the magnetopause is characterized as having only one magnetic source and as being free of plasma. The procedure used here is in many ways similar to the self-consistent field method developed by Mead and Beard to calculate the shape of the magnetopause when the solar wind flow is perpendicular to the dipole axis. They were able to find the surface shape (for perpendicular incidence) at one point at a time. In the present study, however, it is necessary to determine the position of the surface at several points at a time. The geocentric distance to the subsolar point is found to be largest for perpendicular incidence of the solar wind on the dipole axis. The cross sections of the tail of the magnetopause given by the model are not cylindrical but elongated in the direction perpendicular to the ecliptic plane. Generally, the boundary is very dependent upon the wind-dipole angle in the region of the neutral points but exhibits very little dependence on this angle in 'equatorial' regions.

INTRODUCTION

Various attempts have been made to determine the shape of the magnetopause [*Beard*, 1960; *Spreiter and Briggs*, 1961; *Slutz*, 1962; *Midgley and Davis*, 1963; *Mead and Beard*, 1964], which in the closed magnetosphere model is the boundary between the solar wind and the earth's magnetic field. All of the closed magnetosphere models employ similar assumptions. The solar wind is treated as having no random thermal motion (except by Slutz), no associated magnetic field, and as having infinite electrical conductivity. The region within the magnetopause is assumed to be free of plasma and to have the earth's dipole field as its only magnetic source. Because of these assumptions none of the models predicts the formation of the bow shock or the internal features observed in the tail of the magnetosphere. In spite of these limitations the models have been used in many investigations where it is necessary to know the distribution of the magnetic field within the cavity [*Speiser*, 1969; *Reid and Sauer*, 1967; *Roederer*, 1968]. A further limitation in the use of these models is that they treat the case of perpendicular incidence of the solar wind upon the earth's dipole field. In reality the earth's rotation axis makes an angle of 23.5° with the normal to the ecliptic plane. The dipole axis is inclined to the rotation axis by over 11°, thus making the angle between the dipole and the solar wind direction vary annually between 55° and 125°. It is the purpose of this paper to remove the last restriction and determine the magnetopause shape for this range of angles.

THE SELF-CONSISTENT FIELD MODEL OF MEAD AND BEARD

It was found that the self-consistent field method of *Mead and Beard* [1964] could be most easily adapted to make this extension. Their method begins with the pressure balance equation

$$\frac{\mathbf{B}_T \cdot \mathbf{B}_T}{8\pi} = 2nmv^2(\mathbf{v}\cdot\mathbf{n})^2 \qquad (1)$$

which equates the kinetic pressure of the solar wind with the energy density (pressure) of the total magnetic field just inside of the mag-

[1] Based on a portion of a dissertation submitted in partial satisfaction of the requirements for the Ph.D. at the University of California, Los Angeles.

[2] Present address: Space Sciences Department, McDonnell Douglas Astronautics Company—Western Division, Santa Monica, California 90406.

netopause, $\mathbf{B}_T$. Here n is the particle pair density of the solar wind, m is the proton electron pair mass, v is the speed of the wind, $\mathbf{n}$ is the outward unit vector normal to the magnetopause surface, and $\mathbf{v}$ is a unit vector in the solar wind direction. In terms of the coordinate system shown in Figure 1, $\mathbf{n}$ and $\mathbf{v}$ are given as follows

$$\mathbf{n} = a\left[\mathbf{r} - \frac{1}{r}\left(\frac{\partial R}{\partial \theta}\right)\boldsymbol{\theta} - \frac{1}{r\sin\theta}\left(\frac{\partial R}{\partial \phi}\right)\boldsymbol{\phi}\right] \quad (2)$$

where

$$a = \left[1 + \frac{1}{r^2}\left(\frac{\partial R}{\partial \theta}\right)^2 + \frac{1}{r^2\sin^2\theta}\left(\frac{\partial R}{\partial \phi}\right)^2\right]^{-1/2}$$

and $r = R(\theta, \phi)$ is the functional form of the surface and

$$\mathbf{v} = -\cos\theta\mathbf{r} + \sin\theta\boldsymbol{\theta} \quad (3)$$

To guarantee that $\mathbf{B}_T$ is parallel to the magnetopause surface, Mead and Beard suggested that $|\mathbf{B}_T|$ be replaced by $|\mathbf{n} \times \mathbf{B}_T|$. Using this value for $|\mathbf{B}_T|$ and substituting equations 2 and 3 into equation 1 yields a more detailed form of the pressure balance equation

$$\left|\left[\mathbf{r} - \frac{1}{r}\left(\frac{\partial R}{\partial \theta}\right)\boldsymbol{\theta} - \frac{1}{r\sin\theta}\left(\frac{\partial R}{\partial \phi}\right)\boldsymbol{\phi}\right] \times (B_{Tr}\mathbf{r} + B_{T\theta}\boldsymbol{\theta} + B_{T\phi}\boldsymbol{\phi})\right| = (16\pi n m v^2)^{1/2}\left(\cos\theta + \frac{\sin\theta}{r}\frac{\partial R}{\partial \theta}\right) \quad (4)$$

To obtain the shape of the magnetopause, equation 4 is solved for r at a 5° by 5° grid of θ, ϕ values. To do this, however, it is necessary that all quantities appearing in the pressure balance equation must be either known constants or expressible as functions of the position coordinates r, θ, and ϕ. It is noted that n, m, and v are known constants; $\mathbf{v}$ is a function of θ, but *neither* $\mathbf{B}_T$ *nor* $\mathbf{n}$ *can be expressed directly in terms of* r, θ, ϕ.

The representation of $\mathbf{B}_T$. $\mathbf{B}_T$ has two sources, the field from the earth's dipole $\mathbf{B}_G$, and the field generated by currents flowing on the magnetopause, $\mathbf{B}_B$. In component form

$$\mathbf{B}_T = (B_{Gr} + B_{Br})\mathbf{r} + (B_{G\theta} + B_{B\theta})\boldsymbol{\theta} + (B_{G\phi} + B_{B\phi})\boldsymbol{\phi} \quad (5)$$

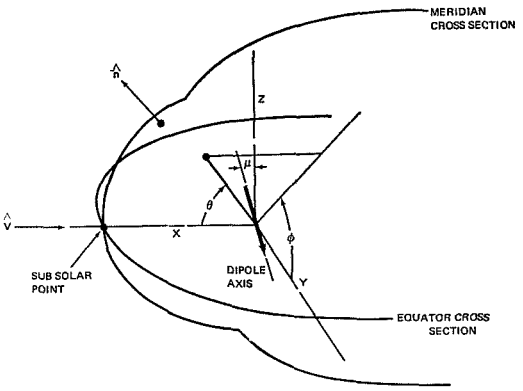

Fig. 1. Coordinate system in which the shape of the magnetopause is determined. The dipole axis is always in the XY plane. $\phi = 0°$ defines the equatorial cross section, while $\phi = 90°$, $-90°$ define the northern and southern portions of the meridian cross section, respectively.

$\mathbf{B}_G$ is known analytically and is expressed as follows

$$B_{Gr} = \frac{M}{r^3}[\cos\theta\,(3A\cos\mu + B\sin\mu) + 3C\sin\theta\cos\phi + (B\cos\mu - 3A\sin\mu)\sin\theta\sin\phi]$$

$$B_{G\theta} = \frac{M}{r^3}[3C\cos\theta\cos\phi + \cos\theta\sin\phi\cdot(B\cos\mu - 3A\sin\mu) - \sin\theta(3A\cos\mu + B\sin\mu)]$$

$$B_{G\phi} = \frac{M}{r^3}[\cos\phi(B\cos\mu - 3A\sin\mu) - 3C\sin\phi]$$

where M is the dipole moment of the geomagnetic field and

$$A = (\cos\mu\cos\theta - \sin\theta\sin\phi\sin\mu)\cdot(\sin\theta\sin\phi\cos\mu + \cos\theta\sin\mu)$$

$$B = 3(\sin\theta\sin\phi\cos\mu + \cos\theta\sin\mu)^2 - 1$$

$$C = \sin\theta\cos\phi\cdot(\sin\theta\sin\phi\cos\mu + \cos\theta\sin\mu)$$

The tilt angle, μ, *is the angle between the dipole axis and the Z axis. The dipole axis is always in*

the XZ plane. Mead and Beard considered the case where the tilt angle is zero. *Beard* [1960] and *Mead and Beard* [1964] argued that although $\mathbf{B}_T(\mathbf{B}_T = \mathbf{B}_G + \mathbf{B}_B)$ is originally unknown (since $\mathbf{B}_B$ cannot be computed until the shape of the magnetopause is known), it can be represented approximately by $2\mathbf{B}_G$. Since $\mathbf{B}_G$ is known analytically, this approximation satisfies the requirement that quantities appearing in the pressure balance equation must be functions of only the coordinates r, θ, ϕ. Using this expression for $\mathbf{B}_T$ and other information relating to $\mathbf{n}$, it is possible to find a 'first surface'—a representation of the shape of the magnetopause.

The representation of $\mathbf{n}$. The normal vector $\mathbf{n}$ is not directly expressible in terms of the position coordinates since it depends upon the two partial derivatives $(\partial R/\partial\theta)$ and $(\partial R/\partial\phi)$ which measure the rate of change in r along constant ϕ and constant θ contours, respectively. It is possible, however, to use finite difference formulas to express each derivative approximately in terms of the values of r at the angular position (θ_0, ϕ_0) where the pressure balance equation is being solved and at two other adjacent values of (θ, ϕ), e.g.

$$\left(\frac{\partial R}{\partial\theta}\right) = (r, r_{-1}, r_{-2}) \tag{6}$$

where r_{-1} and r_{-2} are adjacent points with the same ϕ value as at r but different θ values. Therefore, because of $\mathbf{n}$, the pressure balance equation for a given angular position is dependent not only on the value of r at that position, but also on the values of r at adjacent grid points; the equation cannot be solved unless these other values of r have previously been determined. For perpendicular incidence ($\mu = 0°$), the 'first surface' is determined by *Mead and Beard* [1964] as follows.

Determination of the 'First Surface' for $\mu = 0°$

At the subsolar point (the intersection of the earth-wind line with the magnetopause) both partial derivatives are zero since the surface is planar and perpendicular to r. Therefore, equation 4 reduces to

$$r_0^3 = (M^2/4\pi n\, mv^2)^{1/2}$$

Next, the adjacent point on the equator ($\theta = 5°$, $\phi = 0°$), written (5°, 0°), is examined. Here, $(\partial R/\partial\phi)$ is zero by symmetry. Also, by symmetry, it is known that the value of r on the equator at (5°, 180°) is the same as the r value being determined at (5°, 0°), and equation 4 can be solved. The third r value to be computed is the next one along the equator (10°, 0°). There, the pressure balance equation is immediately expressible in terms of the r values at that grid point since the two previous values of r, needed to express $(\partial R/\partial\theta)$ as a finite difference, have been previously calculated. Consequently, it is possible to determine the entire equator cross section for $\mu = 0°$. The procedure can then be used to compute a ring of points (5°, ϕ) centered on the subsolar point and eventually the entire surface. In fact, *for* $\mu = 0°$, *the entire 'first surface' can be determined one point at a time if three-point finite difference formulas are used to represent* $(\partial R/\partial\theta)$ *and* $(\partial R/\partial\phi)$, except in the antisolar region of the meridian, which will be discussed below.

This, basically, is the procedure used by Mead and Beard. It is possible only because of the symmetry present when the tilt angle is zero. The difficulties encountered when the solar wind flow is not perpendicular to the geomagnetic dipole and the extensions that must be made to overcome them are now discussed.

Determination of 'First Surfaces' for $\mu \neq 0°$

The representation of $\mathbf{B}_T$ is exactly the same as it was for $\mu = 0°$. The representation of $\mathbf{n}$, however, becomes much more complicated due to the diminished amount of symmetry present and the resulting lack of information on the partial derivatives. Along the equator both $(\partial R/\partial\theta)$ and $(\partial R/\partial\phi)$ are unknown. Also, on the meridian there is no point where $(\partial R/\partial\theta)$ is known (although $(\partial R/\partial\phi)$ remains zero). Thus, there is no starting point on the surface where both partial derivatives are known. *It is therefore necessary to solve the pressure balance equation simultaneously at several points.* It is convenient to begin the determination of the shape of the magnetopause along the meridian since $(\partial R/\partial\phi) = 0$ there.

Meridian cross section. Spreiter and Briggs have analytically determined the meridian cross sections in the 'first surface' approximation $(\mathbf{B}_T = 2\mathbf{B}_G)$ for all values of μ. They showed that the meridian is divided into three parts

separated by two singular points at which **n** is discontinuous (see Figure 2). It is therefore necessary to determine these three parts separately. The subsolar point and the two adjacent points (0°, 90°), (5°, 90°), (5°, −90°), referred to as points 1, 2, and 3, respectively, are considered first. The use of finite difference formulas to represent $(\partial R/\partial\theta)$ at each of these three points yields three pressure balance equations

$$F_1(r_1^*, r_2^*, r_3^*) = 0,$$

$$F_2(r_1^*, r_2^*, r_3^*) = 0,$$

$$F_3(r_1^*, r_2^*, r_3^*) = 0$$

where the asterisks indicate the values of r that are roots of the pressure balance equations and the subscripts refer to the three points. At these points, first guesses $r_1^{(1)}$, $r_2^{(1)}$, and $r_3^{(1)}$ are made at the values of r (the superscripts refer to the number of the guess). A correction term β is added to each r value to yield improved estimates, $r_1^{(2)} = r_1^{(1)} + \beta_1^{(1)}$, etc. The values of β are determined by expanding the pressure balance equations in Taylor series and retaining only the linear terms

$$\begin{aligned} F_1(r_1^{(2)}, r_2^{(2)}, r_3^{(2)}) &= F_1(r_1^{(1)}+\beta_1^{(1)}, r_2^{(1)}+\beta_2^{(1)}, r_3^{(1)}+\beta_3^{(1)}) \\ &= F_1(r_1^{(1)}, r_2^{(1)}, r_3^{(1)}) \\ &\quad + \frac{\partial}{\partial r_1}[F_1(r_1^{(1)}, r_2^{(1)}, r_3^{(1)})]\beta_1^{(1)} \\ &\quad + \frac{\partial}{\partial r_2}[F_1(r_1^{(1)}, r_2^{(1)}, r_3^{(1)})]\beta_2^{(1)} \\ &\quad + \frac{\partial}{\partial r_3}[F_1(r_1^{(1)}, r_2^{(1)}, r_3^{(1)})]\beta_3^{(1)} \end{aligned} \tag{7}$$

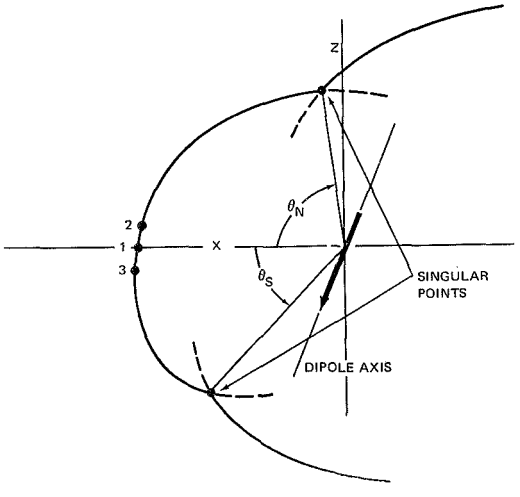

Fig. 2. Determination of meridian cross section.

Similar equations are obtained at points 2 and 3. A system of linear equations results that can be solved for the β's. This process is repeated until the values of F become sufficiently small. $F_1^2 + F_2^2 + F_3^2 < 10^{-20}$ was required. The final values of the r's are taken to be the roots of the pressure balance equations. The shape of the nose portion can then be determined out past the singular points θ_N and θ_S (shown in Figure 2 and computed by Spreiter and Briggs) one point at a time since the preceding two values of r needed to compute $(\partial R/\partial\theta)$ are already known.

To determine the shape of the north meridian beyond the northern singular point the pressure balance equation is again solved simultaneously at three points (their θ values all larger than θ_N). The initial guesses at the values of r are chosen so that they will be closer to the 'tail solution' than the 'nose solution.' (There are only *two* solutions to the pressure balance equation along the meridian in the vicinity of the singular points; everywhere else there is only one. Spreiter's and Brigg's results give two sets of curves from which the proper cross sections are selected by finding the appropriate integration constants. In the present study, the condition of pressure balance is equivalent to their determination of the integration constants.)

A similar procedure is used on the southern meridian. Having found the solutions at the three points on the north and south meridians, the remainder of the tail cross sections can then be determined one point at a time. When this procedure is used for the $\mu = 0°$ meridian, the pressure balance equation can be solved at *every* grid point on the first surface.

Equatorial cross section. Once the meridian cross section has been determined, it is possible to calculate the equatorial cross section by solving the pressure balance equation at three points at a time. If no information were available from the meridian calculation, it would be necessary to solve the pressure balance equation simultaneously at nine points since

TABLE 1. First Surface r Values on the Equator for Various Tilts (v is constant and B_G is dependent on the tilt angle)

	Tilt Angle		
θ, deg	0°	10°	20°
0	1.000	0.998	0.993
20	1.013	1.011	1.007
40	1.054	1.052	1.049
60	1.130	1.130	1.129
80	1.257	1.258	1.253
100	1.470	1.471	1.467
120	1.853	1.852	1.847
140	2.661	2.660	2.650
160	4.980	4.976	

neither $(\partial R/\partial\theta)$ nor $(\partial R/\partial\phi)$ are known there. It is, however, necessary to solve equation 4 simultaneously at the three points $(\theta, 5°)$, $(\theta, 0°)$, $(\theta, -5°)$ for *all values of* θ, since $(\partial R/\partial\phi)$ is not known. $(\partial R/\partial\theta)$ is also unknown but expressible as a function of the r value being determined and other previously determined values of r (constants).

The first surface values of r along the equator are shown for various values of μ in Table 1. For $\mu = 20°$, no r values are given for θ greater than 140° since the pressure balance equations there did not possess roots. This may be attributed to error propagation as θ increases and the approximation to $\mathbf{B}_T$ used to find the first surface. No such problem existed for the 'second surface.' It is seen that the equatorial cross sections are almost independent of the tilt angle, μ. Examination of the pressure balance equation suggests that on the equator for a given value of θ, the dependence of r on the tilt angle is not large. However, it is not readily demonstrated that it is as independent of μ as the results indicate.

Remainder of the surface. Once either the meridian or equatorial cross section of the surface has been determined, it is possible to determine all remaining points on the surface. However, this can be done only with much computational effort. A less complicated yet sufficiently accurate approach is suggested by the following considerations.

All of the r values for $\theta = 90°$ lie in the Y-Z plane (see Figure 1). It is found for the zero tilt surface (which has been obtained by solving the pressure balance equation everywhere) that the magnetopause cross section in the Y-Z plane can quite accurately be represented by an ellipse. In this plane, the r values at the equator, r_E, and on the northern and southern meridians, r_N and r_S, respectively, are always known and sufficient to specify the axis of the ellipse. It is therefore possible to determine all of the remaining r values (for $\theta = 90°$) by fitting an ellipse through r_E, r_N, and r_S. For $\theta \neq 90°$ the values of r are found by fitting ellipses through the projections of r_E, r_N, and r_S (i.e., $r_E \sin\theta$, $r_N \sin\theta$, $r_S \sin\theta$) onto the Y-Z plane. This procedure is used to obtain entire surfaces for μ ranging from 0° to 35° in 5° steps.

Higher-Order Surfaces

Once the shape of a first surface has been determined, the magnitude and direction of the currents flowing on it can readily be computed.

TABLE 2. Geocentric Distances to the 'Second Surface' Representations of the Shape of the Magnetopause for a Tilt Angle of 0°. The distances are given in units of 10 R_E for a 15° by 15° grid of (θ, ϕ) values.

ϕ, deg	θ = 0°	15°	30°	45°	60°	75°	90°	105°	120°	135°	150°	165°
−90	1.0725	1.0766	1.0655	1.0494	1.0175	0.9470	1.2144	1.5257	1.9467	2.6045	3.8706	7.4383
−75	1.0725	1.0764	1.0675	1.0547	1.0273	0.9621	1.2263	1.5333	1.9495	2.6023	3.8476	7.3923
−60	1.0725	1.0760	1.0730	1.0698	1.0555	1.0075	1.2606	1.5548	1.9571	2.5963	3.7868	7.2709
−45	1.0725	1.0754	1.0806	1.0914	1.0982	1.0814	1.3124	1.5856	1.9676	2.5881	3.7083	7.1142
−30	1.0725	1.0748	1.0884	1.1143	1.1465	1.1743	1.3713	1.6183	1.9784	2.5800	3.6344	6.9673
−15	1.0725	1.0743	1.0942	1.1321	1.1862	1.2598	1.4198	1.6435	1.9863	2.5741	3.5830	6.8654
0	1.0725	1.0741	1.0963	1.1388	1.2018	1.2962	1.4388	1.6531	1.9893	2.5720	3.5648	6.8291
15	1.0725	1.0743	1.0942	1.1321	1.1862	1.2598	1.4198	1.6435	1.9863	2.5741	3.5830	6.8654
30	1.0725	1.0748	1.0884	1.1143	1.1465	1.1743	1.3713	1.6183	1.9784	2.5800	3.6344	6.9673
45	1.0725	1.0754	1.0806	1.0914	1.0982	1.0814	1.3124	1.5856	1.9676	2.5881	3.7083	7.1142
60	1.0725	1.0760	1.0730	1.0698	1.0555	1.0075	1.2606	1.5548	1.9571	2.5963	3.7868	7.2709
75	1.0725	1.0764	1.0675	1.0547	1.0273	0.9621	1.2263	1.5333	1.9495	2.6023	3.8476	7.3923
90	1.0725	1.0766	1.0655	1.0494	1.0175	0.9470	1.2144	1.5257	1.9467	2.6045	3.8706	7.4383

TABLE 3. Geocentric Distances to the 'Second Surface' Representations of the Shape of the Magnetopause for a Tilt Angle of 10°. The distances are given in units of 10 R_E radii for a 15° by 15° grid of (θ, ϕ) values.

ϕ, deg	$\theta = 0°$	15°	30°	45°	60°	75°	90°	105°	120°	135°	150°	165°
−90	1.0715	1.0869	1.0882	1.0884	1.0785	1.0403	1.1106	1.4445	1.8667	2.5233	3.7800	7.2363
−75	1.0715	1.0864	1.0896	1.0929	1.0878	1.0529	1.1242	1.4542	1.8722	2.5243	3.7621	7.2027
−60	1.0715	1.0850	1.0932	1.1053	1.1141	1.0899	1.1643	1.4822	1.8878	2.5274	3.7150	7.1141
−45	1.0715	1.0828	1.0976	1.1220	1.1520	1.1473	1.2279	1.5245	1.9112	2.5332	3.6550	7.0010
−30	1.0715	1.0800	1.1007	1.1373	1.1902	1.2149	1.3071	1.5739	1.9389	2.5425	3.6009	6.8985
−15	1.0715	1.0767	1.1005	1.1445	1.2119	1.2728	1.3851	1.6206	1.9666	2.5557	3.5680	6.8355
0	1.0715	1.0733	1.0956	1.1384	1.2017	1.2964	1.4394	1.6539	1.9902	2.5729	3.5656	6.8297
15	1.0715	1.0698	1.0860	1.1182	1.1572	1.2736	1.4536	1.6674	2.0070	2.5933	3.5968	6.8858
30	1.0715	1.0667	1.0730	1.0882	1.0923	1.2163	1.4299	1.6615	2.0163	2.6154	3.6581	7.0003
45	1.0715	1.0640	1.0591	1.0556	1.0261	1.1491	1.3861	1.6431	2.0192	2.6368	3.7390	7.1502
60	1.0715	1.0620	1.0467	1.0273	0.9728	1.0919	1.3421	1.6216	2.0184	2.6548	3.8219	7.3038
75	1.0715	1.0607	1.0384	1.0085	0.9392	1.0550	1.3113	1.6052	2.0165	2.6668	3.8848	7.4203
90	1.0715	1.0603	1.0354	1.0019	0.9278	1.0424	1.3004	1.5992	2.0156	2.6711	3.9084	7.4640

($|\mathbf{J}| = |\mathbf{B}_T|/4\pi$ and $\mathbf{J} = (\mathbf{n} \times \mathbf{B}_T)/4\pi$ where $\mathbf{B}_T = 2\mathbf{B}_G$ on the first surface.) Using the Biot-Savart law, it is possible to integrate over the surface current system and at any point obtain $\mathbf{B}_B$, the magnetic field from these currents. In this integration the surface area elements are represented by trios of points forming triangles instead of using rectangles as was done previously. (Three points define a planar area, whereas four points may not.) The computational details are presented in *Olson* [1968]. $\mathbf{B}_B$ is found at points just inside of the surface and then used in equation 4 to obtain a 'second surface;' i.e., a more accurate representation of the shape of the magnetopause. Here, the equatorial cross section was determined for all values of θ and μ. The procedure for the calculation of the higher-order surfaces is the same as for the second surfaces. Although it has been suggested that the discontinuity in $\mathbf{n}$ (mentioned previously) gives rise to an infinite magnetic field component perpendicular to the surface [*Beard*, 1964], the value of $\mathbf{B}_B$ computed from both first and second surfaces is found to be well-behaved everywhere.

The shapes of the 'second surfaces' are found to provide good representations of the shape of the magnetopause. They are given in tabular form (see Tables 2–5) in terms of the geocentric distances to various angular positions on the surface. These distances are given in units of 10 R_E at a grid of θ, ϕ values for $\mu = 0°$ to 35° in 5° intervals. The negative tilt angle surfaces are then found from symmetry conditions, $r(\theta, \phi, \mu) = r(\theta, -\phi, -\mu)$.

Comparisons and Checks

The predictions of the present model are compared with earlier results whenever possible. *Spreiter and Briggs* [1961] were able to obtain

TABLE 4. Geocentric Distances to the 'Second Surface' Representations of the Shape of the Magnetopause for a Tilt Angle of 20°. The distances are given in units of 10 R_E for a 15° by 15° grid of (θ, ϕ) values.

ϕ, deg	$\theta = 0°$	15°	30°	45°	60°	75°	90°	105°	120°	135°	150°	165°
−90	1.0680	1.0852	1.1032	1.1192	1.1286	1.1300	1.0912	1.3342	1.7638	2.4149	3.6522	6.9630
−75	1.0680	1.0849	1.1044	1.1234	1.1359	1.1392	1.1048	1.3470	1.7731	2.4207	3.6415	6.9440
−60	1.0680	1.0841	1.1072	1.1347	1.1562	1.1654	1.1449	1.3846	1.8001	2.4375	3.6139	6.8952
−45	1.0680	1.0824	1.1098	1.1486	1.1838	1.2045	1.2094	1.4436	1.8416	2.4640	3.5806	6.8370
−30	1.0680	1.0795	1.1098	1.1583	1.2089	1.2478	1.2911	1.5172	1.8925	2.4979	3.5550	6.7943
−15	1.0680	1.0754	1.1046	1.1560	1.2181	1.2830	1.3754	1.5933	1.9457	2.5364	3.5487	6.7882
0	1.0680	1.0699	1.0929	1.1366	1.2011	1.2971	1.4413	1.6567	1.9936	2.5765	3.5689	6.8324
15	1.0680	1.0634	1.0752	1.1010	1.1575	1.2846	1.4712	1.6952	2.0304	2.6150	3.6178	6.9304
30	1.0680	1.0565	1.0539	1.0561	1.0986	1.2507	1.4639	1.7059	2.0534	2.6493	3.6914	7.0749
45	1.0680	1.0499	1.0324	1.0114	1.0394	1.2083	1.4335	1.6960	2.0643	2.6774	3.7795	7.2460
60	1.0680	1.0445	1.0142	0.9747	0.9914	1.1699	1.3985	1.6779	2.0669	2.6980	3.8653	7.4119
75	1.0680	1.0409	1.0021	0.9510	0.9609	1.1439	1.3726	1.6623	2.0662	2.7106	3.9287	7.5340
90	1.0680	1.0397	0.9979	0.9429	0.9505	1.1348	1.3632	1.6564	2.0655	2.7148	3.9522	7.5791

TABLE 5. Geocentric Distances to the 'Second Surface' Representations of the Shape of the Magnetopause for a Tilt Angle of 30° The distances are given in units of 10 R_E for a 15° by 15° grid of (θ, ϕ) values.

ϕ, deg	$\theta = 0°$	15°	30°	45°	60°	75°	90°	105°	120°	135°	150°	165°
−90	1.0586	1.0876	1.1128	1.1405	1.1686	1.1936	1.2067	1.2159	1.6526	2.2942	3.5065	6.6545
−75	1.0586	1.0871	1.1139	1.1454	1.1735	1.1998	1.2168	1.2315	1.6659	2.3053	3.5043	6.6525
−60	1.0586	1.0855	1.1163	1.1581	1.1868	1.2171	1.2461	1.2782	1.7049	2.3377	3.4999	6.6503
−45	1.0586	1.0824	1.1177	1.1728	1.2037	1.2421	1.2915	1.3543	1.7662	2.3882	3.4987	6.6571
−30	1.0586	1.0774	1.1148	1.1797	1.2167	1.2686	1.3465	1.4540	1.8433	2.4512	3.5077	6.6849
−15	1.0586	1.0702	1.1044	1.1679	1.2159	1.2892	1.4013	1.5638	1.9259	2.5197	3.5331	6.7444
0	1.0586	1.0609	1.0853	1.1310	1.1981	1.2971	1.4442	1.6623	2.0013	2.5856	3.5786	6.8417
15	1.0586	1.0502	1.0585	1.0729	1.1612	1.2894	1.4668	1.7282	2.0587	2.6421	3.6443	6.9762
30	1.0586	1.0389	1.0279	1.0059	1.1136	1.2690	1.4684	1.7535	2.0929	2.6850	3.7257	7.1392
45	1.0586	1.0282	0.9981	0.9435	1.0656	1.2425	1.4553	1.7475	2.1067	2.7137	3.8134	7.3124
60	1.0586	1.0196	0.9736	0.8950	1.0262	1.2176	1.4373	1.7276	2.1076	2.7304	3.8935	7.4692
75	1.0586	1.0139	0.9576	0.8649	1.0008	1.2003	1.4229	1.7093	2.1041	2.7386	3.9503	7.5798
90	1.0586	1.0119	0.9521	0.8548	0.9921	1.1942	1.4175	1.7022	2.1022	2.7409	3.9709	7.6198

analytically the first surface meridian cross sections for all tilt angles. A comparison of the two sets of results indicates that for all tilt angles the meridian cross sections are identical to four significant figures. Because of this, the first surface meridian values of r are not shown here.

This excellent agreement suggests that the method used here is valid for all tilt angles and that the three-point finite difference formula used to represent $(\partial R/\partial\theta)$ and the angular distances between grid points are appropriate and do not introduce appreciable errors. Also it shows, for all values of μ, that the pressure balance equation can be solved at all points on the meridian *including the antisolar portion.*

For $\mu = 0°$ (see Table 3) the 'second surface' can be compared with the 'final surface' reported by *Mead and Beard* [1964] (see their Table 1, p. 1175). Along the equator, the differences in the r values for θ less than 150° are no more than 2% of the r values obtained by Mead and Beard. The differences in the meridian r values are also less than 2% for θ less than 150°, except in the region of the neutral points. Generally, the two surfaces are very similar in both size and shape. This agreement again indicates that the present method provides an appropriate representation of the magnetopause surface.

The accuracy of the ellipse fitting method was tested by comparing the surfaces obtained by

TABLE 6. Comparison of r Values from Ellipse Fitting Model (EL) with Those Obtained by Solving the Pressure Balance Equation Point by Point (PB)

	$\theta = 5°$		$\theta = 15°$		$\theta = 25°$		$\theta = 35°$		$\theta = 45°$	
ϕ, deg	EL	PB	EL	PB	EL	PB	EL	PB	EL	PB
−90	0.988	0.988	0.978	0.978	0.967	0.967				
−75	0.989	0.988	0.979	0.979	0.970	0.971				
−60	0.991	0.989	0.983	0.983	0.977	0.979				
−45	0.993	0.990	0.989	0.988	0.988	0.989				
−30	0.996	0.991	0.996	0.993	1.000	0.999				
−15	0.999	0.993	1.002	0.998	1.011	1.008				
0	1.001	0.994	1.007	1.002	1.020	1.015				
15	1.002	0.995	1.011	1.005	1.025	1.019				
30	1.001	0.996	1.012	1.007	1.026	1.021				
45	1.001	0.997	1.012	1.008	1.025	1.020				
60	0.999	0.998	1.011	1.009	1.022	1.019				
75	0.999	0.998	1.011	1.010	1.019	1.018	1.031	1.031	1.045	1.043
90	0.998	0.998	1.010	1.010	1.018	1.018	1.030	1.030	1.041	1.041

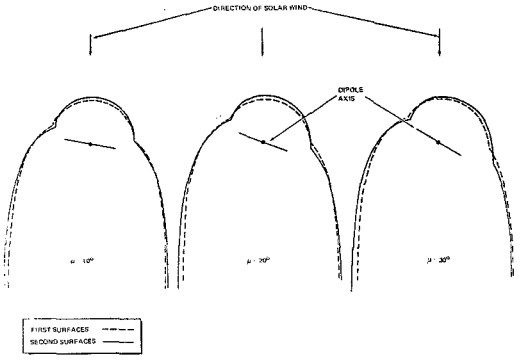

Fig. 3. First and second surface meridian cross sections for various tilt angles. (First surface cross sections are identical to those obtained by *Spreiter and Briggs* [1961].)

fitting ellipses with portions of the surfaces obtained by solving the pressure balance equation point by point. An example of this comparison is given for an intermediate tilt angle ($\mu = 20°$) in Table 6.

It is observed that the r values predicted by the two methods never differ by more than 0.06 R_E (less than 0.7% of the correct value of r), again indicating that the numerical procedures used provide a good representation of the shape of the magnetopause.

Description of the Tilted Surfaces

General description. The inclusion of the boundary current field, $\mathbf{B}_B$, in the estimate of the total field, $\mathbf{B}_T$, in general causes the second surfaces to be slightly larger than the first. The subsolar point and meridian r values increase for all values of μ by about 7%. As seen in Figure 3, the meridian r values also increase except in the vicinity of the neutral points.

TABLE 7. Variation in the Subsolar Distance with Tilt Angle

μ, deg	First Surface	Second Surface
0	1.000	1.072
5	1.000	1.072
10	0.998	1.072
15	0.996	1.070
20	0.993	1.068
25	0.989	1.063
30	0.985	1.059
35	0.979	1.045

Cross sections of the tail for all tilt angles are not circular. A more detailed description follows.

Subsolar point. It has been suggested that as the absolute value of the tilt angle increases, the geocentric distance to the subsolar point will increase by up to 12% [*Patel and Dessler*, 1966], or decrease by up to 7% [*Schield*, 1969]. In the present model the subsolar distance decreases with increasing tilt angle, thereby supporting Schield (see Table 7). However, the model suggests that the decrease in r (for μ going from 0° to 35°) will be under 3%, less than half of Schield's prediction.

That the subsolar distance should decrease with increasing tilt angle and at a rate less than that suggested by Schield can be seen by examining the pressure balance equation (equation 1). $\mathbf{B}_T$ is the total field tangent to the magnetopause at the subsolar point and in the first surface approximation is given by $2\mathbf{B}_G$. In the coordinate system shown in Figure 4, $\mathbf{B}_G$ has components $B_r = -2M/r^3 \sin \mu$ and $B_\mu = M/r^3 \cos \mu$. $\mathbf{B}_T$ consists of the projections of these components onto the magnetopause surface. They are $B_\mu \cos \xi$ and $B_r \sin \xi$ where ξ is the angle between the earth-wind line (X axis) and the normal to the surface. After normalization equation 1 becomes

$$r^6 = \cos^2 \mu + 4 \sin \mu \cos \mu \tan \xi + 4 \sin^2 \mu \tan^2 \xi \qquad (8)$$

For $\mu = 35°$, ξ is about 6°, and the terms of

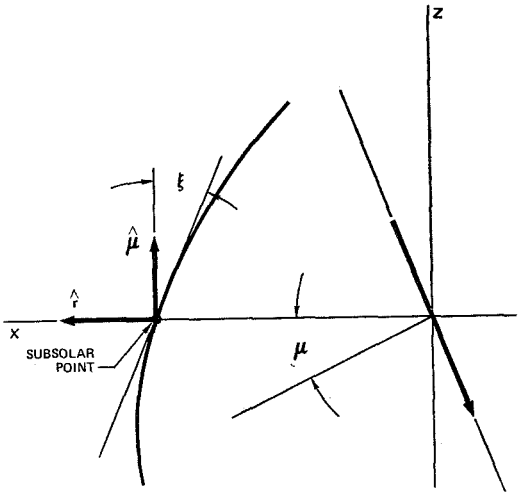

Fig. 4. Determination of the subsolar distance.

TABLE 8. Coordinates of the Neutral Points for Several Values of μ

R_N and R_S are in earth radii.

μ, deg	R_N	θ_N	R_S	θ_S
0	9.38	74.0	9.38	74.0
5	9.27	70.1	9.54	78.3
10	8.86	66.0	9.65	82.9
15	8.67	62.8	10.28	88.0
20	8.48	55.0	10.65	93.1
25	8.29	51.2	11.31	100.0
30	8.24	49.1	12.10	104.3
35	8.21	44.7	12.68	109.1

equation 8 are (in order)

$$r^6 = 0.6710 + 0.1975 + 0.0145$$

Thus the term containing tan ξ is appreciable and accounts for the 3% instead of the 7% decrease.

If the meridian cross section in the vicinity of the subsolar point remained circular for all μ, ξ would be zero, and equation 8 would reduce to the form used by Schield. Simply using the total field $2\mathbf{B}_G$ (not the portion of it parallel to the boundary) overestimates the pressure from $\mathbf{B}_G$ and incorrectly increases the boundary distance.

Neutral points. As is seen in Figure 3, the discontinuity in the $\mathbf{n}$ in the vicinity of the neutral points is larger on the second surface (when the field from the boundary currents is included in the estimate of $\mathbf{B}_T$), i.e., the neutral points are more indented. The geocentric distances and angular positions of the neutral points are given in Table 8 for both first and second surfaces. The r values increase monotonically with increasing μ for the southern neutral point to a maximum value of 12.68 r_E for $\mu = 35°$ and decrease to a minimum of 8.21 r_E at $\mu = 35°$ for the northern neutral point. The angular coordinates θ_S and θ_N (see Figure 2) increase monotonically with μ, whereas λ_S and λ_N, the angular distances between the neutral points and the dipole axis, remain almost constant.

For the second surface λ_S varies between 15° and 17°, and λ_N ranges from 16° at $\mu = 0°$ down to 10° when $\mu = 35°$. This dependence of λ on μ is much less than that for the first surface where λ_N ranges from 19° to 12° and λ_S varies from 19° to 24°. This suggests that the magnetic field line extending from the neutral points to the dipole origin always intersects the earth's surface at almost the same latitude and does not vary appreciably with the tilt angle.

Equator. The second surface equatorial cross sections show only a slight dependence on the tilt angle. They are from 5% to 8% larger than the corresponding first surface equatorial cross sections but almost identical to them in shape.

Tail cross section. The geocentric distances to the boundary for $\theta = 165°$ on the equator and the northern and southern branches of the meridian are given in Table 9. It is seen that for all values of μ the boundary is no cylindrical but elongated in the direction perpendicular to the ecliptic (X-Y) plane. This is similar to the geometry observed by *Behannon* [1968]. Notice also that as the tilt angle increases (positively) the center of the tail cross section is raised above the ecliptic plane. This is the same as the direction the neutral sheet is observed to move as the tilt angle increases [*Speiser and Ness*, 1967].

Magnetic Fields from Magnetopause Currents

The field from the magnetopause currents, $\mathbf{B}_B$, can be found anywhere within the magnetopause. In particular, the field distribution at the earth's surface can be studied. However, near the earth, $\mathbf{B}_B$ will be distorted by induction currents flowing within the earth and masked by the fields produced by ionospheric currents.

TABLE 9. Variation of Cross-Sectional Shape of the Tail of the Magnetopause for Several Values of μ

All distances (geocentric) are given in earth radii and are for $\theta = 165°$.

Tilt Angle μ, deg	North Meridian, $\theta = \pi/2$	Equator, $\theta = 0$	South Meridian, $\theta = -\pi/2$
0	74.39	68.29	74.39
5	73.70	68.29	73.36
10	74.64	68.30	72.36
15	75.19	68.31	71.04
20	75.79	68.32	69.63
25	76.11	68.37	68.07
30	76.20	68.42	66.55
35	76.00	68.56	64.75

At geosynchronous altitude, these problems should not occur. As magnetometer data become available from the geosynchronous satellite ATS 1, it will be possible to test the model presented here. It is expected that in the vicinity of the noon meridian the agreement will be good, whereas near the midnight meridian differences probably will occur as a result of the neutral sheet currents.

Summary and Conclusions

A model has been developed that represents the shape of the magnetopause for all angles of incidence of the solar wind upon the earth's dipole axis. Although several assumptions are made in the model and further simplifications are employed in its development, the surfaces predicted by it are found to be in agreement with those obtained by other models whenever comparisons can be made. The entire second surface for $\mu = 0°$ agrees well with the final surface obtained by Mead and Beard, whereas the first surface meridian cross sections are in excellent agreement with the results of Spreiter and Briggs.

The equatorial cross sections are found to be almost independent of the tilt angle, whereas the meridian cross sections are highly dependent upon the tilt angle. The positions of the neutral points vary with μ and are significantly different from those predicted by the 'zero tilt' models. The shape of the magnetopause for various tilt angles is given in Tables 2–5. Geocentric distances are given in earth radii for a grid of (θ, ϕ) values.

This model can be used to calculate quantitatively the spatial distribution and temporal variations in the magnetic field produced by the magnetopause current system. It will predict seasonal variations in addition to yielding improved values for the daily variations. To the extent that these variations are important, and accuracy in the calculation of the magnetospheric magnetic field is required, this model is a considerable improvement over the existing 'zero tilt' models.

Acknowledgments. The author was supported by a Ford Foundation fellowship and a NASA traineeship during the period in which this study was done. He wishes to thank Professor G. J. F. MacDonald for his guidance and Professor S. V. Venkateswaran for his constant help and encouragement. Professor E. H. Vestine also made several useful suggestions, and Mr. D. E. St. John provided valuable assistance with the programming effort.

Final preparation was supported by the McDonnell Douglas Independent Research and Development program.

References

Beard, D. B., The interaction of the terrestrial magnetic field with the solar corpuscular radiation, *J. Geophys. Res., 65,* 3559, 1960.

Beard, D. B., The solar wind geomagnetic field boundary, *Rev. Geophys., 2,* 335, 1964.

Behannon, K. W., Mapping of the earth's bow shock and magnetic tail by Explorer 33, *J. Geophys. Res., 73,* 907, 1960.

Mead, G. D., and D. B. Beard, Shape of the geomagnetic field-solar wind boundary, *J. Geophys. Res., 69,* 1169, 1964.

Midgley, J. E., and L. Davis, Jr., Calculation by a moment technique of the perturbation of the geomagnetic field by the solar wind, *J. Geophys. Res., 68,* 5111, 1963.

Ness, N. F., C. S. Searce, and J. B. Seek, Initial results of the Imp I magnetic field experiment, *J. Geophys. Res., 69,* 3531, 1964.

Olson, W. P., The magnetopause surfaces and fields for various inclinations of the earth's dipole axis to the solar wind, dissertation, University of California, Los Angeles, 1968.

Patel, V. L., and A. J. Dessler, Geomagnetic activity and size of magnetospheric cavity, *J. Geophys. Res., 71,* 1940, 1966.

Reid, G. C., and H. H. Sauer, The influence of the geomagnetic tail on low-energy, cosmic-ray cutoffs, *J. Geophys. Res., 72,* 197, 1967.

Roederer, J. G., Shell splitting and radial diffusion of geomagnetically trapped particles, in *Earth's Particles and Fields,* edited by B. M. McCormac, p. 193, Reinhold Publishing Corp., New York, 1968.

Schield, M. A., Pressure balance between solar wind and magnetosphere, *J. Geophys. Res., 74,* 1275, 1969.

Slutz, R. J., The shape of the geomagnetic field boundary under uniform external pressure, *J. Geophys. Res., 67,* 505, 1962.

Speiser, T. W., Some recent results using the Dungey model, in *Atmospheric Emissions,* edited by B. M. McCormac, Reinhold Publishing Corp., New York, 1969.

Speiser, T. W., and N. F. Ness, The neutral sheet in the geomagnetic tail: Its motion, equivalent currents and field line connection through it, *J. Geophys. Res., 72,* 131, 1967.

Spreiter, J. R., and B. R. Briggs, Theoretical determination of the form of the hollow produced in the solar corpuscular stream by interaction with the magnetic dipole field of the earth, *NASA Rept. R-120,* 1961.

(Received April 21, 1969;
revised July 11, 1969.)